The current issue and full text archive of this journal is available at
www.emeraldinsight.com/0961-5539.htm

Received November 2005
Revised April 2006
Accepted April 2006

Finite point based numerical study on the unsteady laminar wake behind square cylinders

B. Mendez
Instituto Universitario Ignacio da Riva,
Universidad Politecnica de Madrid, Madrid, Spain, and
A. Velazquez
Propulsion and Fluid Mechanics Department, School of Aeronautics,
Universidad Politecnica de Madrid, Madrid, Spain

Abstract

Purpose – The purpose of this paper is to present numerical study on the behaviour of 2D unsteady incompressible laminar wakes behind square cylinders.

Design/methodology/approach – The numerical method that has been developed is based on a finite point formulation characterised by its weak connectivity requirements. This formulation allows for a patched unstructured approach to computational domain modelling that is of interest for industrial applications. Time evolution of pressure is computed by using a pseudo-compressibility relaxation model that is based on physical considerations.

Findings – This model is characterised by the fact that no sub-iterations on a numerical pseudo-time are required so that computational efficiency is increased. Algorithm stability requires the use of second and fourth order artificial viscosity operators that effectively change the order of the equations. A discussion is included regarding the boundary conditions for these operators that do not influence vortex shedding behaviour.

Research limitations/implications – Bearing in mind the industrial drive (MEMS design) that the authors have in mind, solver validation has been addressed at two levels: global coefficients (lift, drag and Strouhal number) were compared with those published in the specialised literature, while local velocity and rms profiles were compared with those obtained after performing a specific low velocity wind tunnel testing campaign (Reynolds numbers in the range from 110 to 268).

Practical implications – A sensitivity analysis of the results obtained is presented and it shows that the solver numerical robustness makes it amenable for project oriented applications.

Originality/value – The formulation being presented is competitive and could be considered as a potential alternative to other approaches.

Keywords Flow, Numerical analysis

Paper type Research paper

Introduction

Micro-electro-mechanical systems (MEMS) design and manufacturing is a growing engineering field that is beginning to make an impact on quite a number of industrial

---

The authors want to thank Prof. J. Meseguer, Head of Instituto Universitario Ignacio da Riva (IDR), for providing the experimental facilities, also, for his useful comments and indications. The authors are also grateful to the technicians at IDR: Rafael Garcia, Alejandro Martinez and Javier Pascual, for their invaluable help to perform the wind tunnel testing.

International Journal of Numerical Methods for Heat & Fluid Flow
Vol. 17 No. 1, 2007
pp. 108-132
© Emerald Group Publishing Limited
0961-5539
DOI 10.1108/09615530710716108

sectors such as, for instance, space, aeronautics, and defence. Furthermore, the fact that the MEMS sector has not reached maturity means that there is opportunity for the exploration of new ideas and concepts. In particular, there is a very large class of MEMS that rely on fluid and/or thermal phenomena, and it is likely that the number and sophistication of these thermo-fluid devices will increase dramatically. Then, it is important to develop prediction and design tools that are simultaneously flexible, reliable and robust, and that target the flow regimes that typically occur inside these industrial products.

Depending on the flow regime and flow parameters, and on the specific characteristics of the problem under consideration, either the continuum approach (i.e. the Navier-Stokes equations) or the Boltzmann equation should be used. A comprehensive discussion on the different regimes to be expected inside MEMS, including the usefulness of using the classical continuous approach, been recently published by Stone *et al.* (2004). For example, a practical application of the Navier-Stokes equations to evaluate heat transfer inside a gas phase micro-reactor has been reported recently by Van Male *et al.* (2004). Here, the authors studied gas flow at Reynolds number of the order of 200 inside micro-channels whose square cross-section was $500 \times 500\,\mu$m. On the other hand, a Boltzman equation based study of gas flow inside a different micro-fluidics system has been published by Chung (2005). In this case, the channel cross-section was $0.5 \times 15\,\mu$m and this, together with the flow conditions at the entrance, justified the use of the kinetic theory formulation. The work presented hereafter deals with the application of the continuous approach.

In this context, so-called gridless and/or meshless numerical methods are potential candidates to be considered practical design tools because of their aim to relax, step by step, the requirements of traditional finite differences, elements or volumes approaches that, needless to say, are also significantly evolving on their own. Finite point methods, that could be considered a particular case of meshless methods, use clouds of points that cover the computational domain in an unstructured way. Connectivity between points is weak and this fact allows for the possibility of patching up the flow field with regions that have markedly different densities of points. The idea of scattering points around the computational domain dates back to the seventies. To the knowledge of the authors of this paper, first results were reported by Jensen (1972) and Perrone and Kao (1975), while the next series of improvements were published by Liszka and Orkisz (1980). One of the first steady-state Euler/Navier-Stokes finite points algorithms that could be used for industrial applications in the aerospace field was published by Batina (1992). Some recent developments in the field have been published by Luo and Haussler-Combe (2002), Li and Aluru (2002), Onate *et al.* (1996), Ding *et al.* (2004) and Mendez and Velazquez (2004).

Finite point methods look promising in the field of industrial applications because of both their efficiency to address complex computational domain discretisation and inherent numerical robustness. At the same time, they are not as computationally time-efficient as other methods; however, the current trend of ever lowering CPU prices in the computer industry can readily make up for this drawback. As it could be expected, loss of computational time-efficiency could be traced back to the avoidance of strong requirements for geometry modelisation. Derivatives are often computed by making a least squares approximation within the cloud, so that accuracy and time needed to compute them grows along with the number of points accounted for. A close-up view of a typical mesh for computation of the flow around a square cylinder is shown in Figure 1 where a series of patches could be seen that cover the computational domain. In an ideal situation, clouds used to compute derivatives should

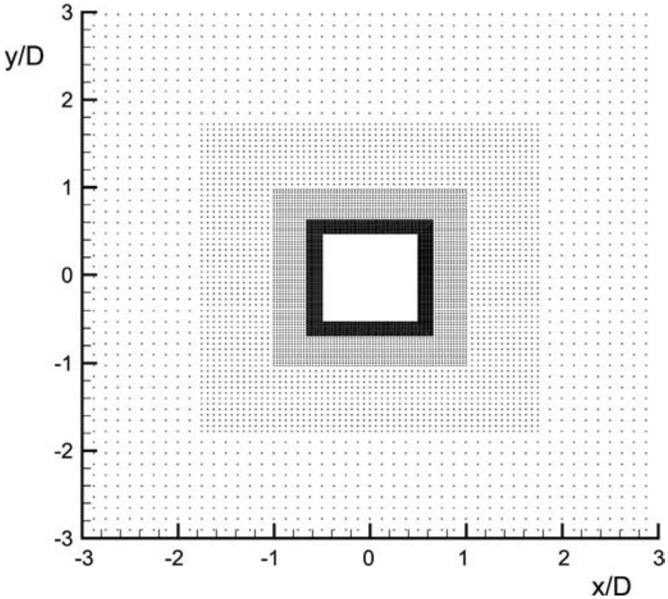

Figure 1.
Close-up view of a typical finite point computational domain around a square cylinder

contain more points in the transition regions between patches than inside the patches themselves. However, to keep formulation simple, most fine point solvers use the same number of points inside the clouds regardless of their location.

The work presented in this paper deals with the development and application of a finite point solver to the problem of predicting unsteady laminar wake behaviour behind square cylinders. In a previous paper, Mendez and Velazquez (2004) have described solver formulation and sensitivity of the solutions with regard to the different artificial viscosity parameters. Validation was performed by comparing with global aerodynamics coefficients (drag, lift and Strouhal number) that could be found in the specialised literature. The work presented in the present paper goes a step further in the sense that it focuses on the prediction of local variables (velocity profiles and rmss in the cylinder wake). Also, it re-formulates cloud definition and artificial viscosity terms so as to gain computational efficiency without loss of accuracy. Additionally, it studies the effect that boundary conditions for the artificial viscosity operators (needed for stability) have on vortex shedding behaviour. Although it is not often recognised, numerical viscosity operators actually increase the order of the equations being solved and, therefore, require the implementation of appropriate higher order boundary conditions. The effect is barely noticeable when dealing with steady flows but, as it happens in our case, the influence of the higher order boundary conditions is critical when unsteady problems are considered. Regarding solver validation, local velocity profiles and rms's at the wake used for comparison purposes have been obtained by performing an experimental campaign in a low velocity wind tunnel (Reynolds number in the range 110-268). Hot wire anemometry was used to build up the experimental data bases. Regarding paper organisation, the work is presented in the shape of consecutive chapters that deal with: governing equations, space and time discretisation, artificial dissipation, validation, wake results, sensitivity of results, and conclusions.

Flow equations

Governing equations of the problem are:

$$\frac{\partial \hat{p}}{\partial \hat{t}} + \beta\left(\frac{\partial \hat{u}}{\partial \hat{x}} + \frac{\partial \hat{v}}{\partial \hat{y}}\right) + \hat{u}\frac{\partial \hat{p}}{\partial \hat{x}} + \hat{v}\frac{\partial \hat{p}}{\partial \hat{y}} = 0 \tag{1}$$

$$\frac{\partial \hat{u}}{\partial \hat{t}} + \hat{u}\frac{\partial \hat{u}}{\partial \hat{x}} + \hat{v}\frac{\partial \hat{u}}{\partial \hat{y}} = -\frac{\partial \hat{p}}{\partial \hat{x}} + \frac{1}{Re}\left(\frac{\partial^2 \hat{u}}{\partial \hat{x}^2} + \frac{\partial^2 \hat{u}}{\partial \hat{y}^2}\right) \tag{2}$$

$$\frac{\partial \hat{v}}{\partial \hat{t}} + \hat{u}\frac{\partial \hat{v}}{\partial \hat{x}} + \hat{v}\frac{\partial \hat{v}}{\partial \hat{y}} = -\frac{\partial \hat{p}}{\partial \hat{y}} + \frac{1}{Re}\left(\frac{\partial^2 \hat{v}}{\partial \hat{x}^2} + \frac{\partial^2 \hat{v}}{\partial \hat{y}^2}\right) \tag{3}$$

where dimensionless pressure $\hat{p}$, velocities $\hat{u}, \hat{v}$, spatial co-ordinates $\hat{x}, \hat{y}$, and time $\hat{t}$, are defined as follows:

$$\hat{p} = \frac{p - p_\infty}{\rho_\infty u_\infty^2}, \quad \hat{u} = \frac{u}{u_\infty}, \quad \hat{v} = \frac{v}{u_\infty}, \quad \hat{x} = \frac{x}{L}, \quad \hat{y} = \frac{y}{L}, \quad \hat{t} = \frac{u_\infty t}{L} \tag{4}$$

Subscript ∞ denotes upstream unperturbed conditions, L stands for the characteristic length of the problem (cylinder diameter) and ρ designates density. Re is the Reynolds number of the problem and β is a pseudo-compressibility parameter to be described in the following.

Equation (1) originates from the continuity equation:

$$\frac{\partial \rho}{\partial t} + \vec{\nabla}\cdot(\rho\vec{v}) = 0 \tag{5}$$

The flow regime that we consider is characterised by the fact that density and pressure variations are very small compared to density and pressure themselves, so we write:

$$p = p_\infty + \Delta p \tag{6}$$

$$\rho = \rho_\infty + \Delta\rho \tag{7}$$

When taking gas state equation into account (γ is the specific heat ratio) together with relations (6) and (7), continuity equation (5) could be written as:

$$\frac{\gamma}{a_\infty^2}\,\frac{\partial(p - p_\infty)}{\partial t} + \rho_\infty\vec{\nabla}\cdot\vec{v} + \frac{\gamma}{a_\infty^2}\vec{v}\cdot\vec{\nabla}(p - p_\infty) = 0 \tag{8}$$

where a_∞ is the sound velocity. Equation (8) is made dimensionless by using relations (4) as follows:

$$\frac{\partial \hat{p}}{\partial \hat{t}} + \alpha(\vec{\nabla}\cdot\hat{\vec{v}}) + \hat{\vec{v}}\cdot\vec{\nabla}\hat{p} = 0 \tag{9}$$

where α (the so-called compressibility coefficient) is defined as:

$$\alpha = \frac{1}{\gamma}\left(\frac{a_\infty}{u_\infty}\right)^2 \tag{10}$$

Typical values of α are very large. For instance, in a wind tunnel experiment where $u_\infty = 1\,\text{m/s}$, α is of the order of 10^5. Since, α is so large compared to unity, the usual procedure is to retain the leading term in equation (9) so that continuity equation reduces to:

$$(\vec{\nabla} \cdot \hat{\vec{v}}) = 0 \tag{11}$$

Equation (9) is very interesting from the computational point of view because it represents a physical model and, also, because it contains the time derivative of pressure. The downside is that the very large value of α imposes strong restrictions on the stability of numerical algorithms that attempt to solve this equation. Our approach consists on using a pseudo-compressibility coefficient β that is smaller than the physical compressibility coefficient α but that still is much larger than unity. In this way we relax the stability requirements of the numerical algorithm while retaining the main physical aspects of the problem:

$$\alpha \gg \beta \gg 1 \tag{12}$$

Accordingly, the equation that we actually solve is:

$$\frac{\partial \hat{p}}{\partial \hat{t}} + \beta(\vec{\nabla} \cdot \hat{\vec{v}}) + \hat{\vec{v}} \cdot \vec{\nabla}\hat{p} = 0 \tag{13}$$

Equation (13) can be integrated on the physical dimensionless time $\hat{t}$, so the implementation of a computational pseudo-time is not required, as it happens in other formulations such a the original one reported by Chorin (1967). In practice, we are able to use an explicit time integration scheme because we relax the incompressibility constrain. Obviously, this is not a merit on itself and the possible advantages obtained regarding simplified coding of the algorithm and numerical robustness should be weighted against accuracy and required CPU time. What we found is that, when considering practical engineering design applications, the formulation that we use is competitive and it could be considered as a potential alternative to other approaches.

The main numerical issue with equation (13) is the selection of the pseudo-compressibility parameter β. This parameter needs to be selected for the flow Reynolds number regime being considered. Mendez and Velazquez (2004) performed a sensitivity analysis of the simulation results with regard to β and showed that, for the range of Reynolds numbers being considered hereafter, a reasonable value is 100. This result agrees with the findings provided by other researchers, such as Kiris and Kwak (2002), who use the standard pseudo-compressibility formulation. When using the pseudo-compressibility method, one actually solves the limit Mach → 0 and, in fact, the results should be independent of β. This subject has been discussed at some length by Rogers *et al.* (1991), and this is the reason why Mendez and Velazquez (2004), after having studied the sensitivity of the results with regard to β, have selected the value of 100 as the operative one.

Regarding initial conditions, the flow is supposed to be uniform at $\hat{t} = 0$. This means that we do not study the transient regime that takes place until the oscillatory permanent regime is achieved.

Boundary conditions are:

$$\hat{u} = 1, \;\; \hat{v} = 0, \;\; \frac{\partial \hat{p}}{\partial \hat{n}} = 0, \;\; \text{at inlet section} \tag{14}$$

$$\frac{\partial \hat{u}}{\partial \hat{n}} = 0, \;\; \frac{\partial \hat{v}}{\partial \hat{n}} = 0, \;\; \frac{\partial \hat{p}}{\partial \hat{n}} = 0, \;\; \text{at outlet section} \tag{15}$$

where $\hat{n}$ is the normal to the section surface:

$$\hat{u} = 0, \ \hat{v} = 0, \ \frac{\partial \hat{p}}{\partial \hat{x}} = \frac{1}{Re}\left(\frac{\partial^2 \hat{u}}{\partial \hat{x}^2} + \frac{\partial^2 \hat{u}}{\partial \hat{y}^2}\right), \ \text{at vertical walls} \tag{16}$$

$$\hat{u} = 0, \ \hat{v} = 0, \ \frac{\partial \hat{p}}{\partial \hat{y}} = \frac{1}{Re}\left(\frac{\partial^2 \hat{v}}{\partial \hat{x}^2} + \frac{\partial^2 \hat{v}}{\partial \hat{y}^2}\right), \ \text{at horizontal walls} \tag{17}$$

In principle, whenever $Re \gg 1$, equations (16) and (17) lead to the boundary condition $\partial \hat{p}/\partial \hat{n} = 0$ that has sometimes been used in the literature. However, it is to be noted that this condition may not be true when the velocity gradient is also large. Relations (16) and (17) can also be easily re-formulated when curved walls are considered.

An alternative to boundary conditions (16) and (17) is to solve momentum equations at the wall (using one sided derivatives) so that the contribution from the convective terms is accounted for. This issue is discussed in detail in the validation section of this paper where computations obtained by using the different boundary conditions are evaluated and compared between themselves.

Space and time integration

The functional approximation $f(\hat{x},\hat{y})$ used to describe local behavior of the flow variables is:

$$f(\hat{x},\hat{y}) = f_0 + \lambda_1\hat{x} + \lambda_2\hat{y} + \lambda_3\hat{x}^2 + \lambda_4\hat{y}^2 + \lambda_5\hat{x}\hat{y} \tag{18}$$

The λ_i coefficients for the velocity components and pressure are obtained by using a least square approach in a cloud of points surrounding the central point where integration is to be carried out. Formulation (18) makes sure that the least squares functional approach passes trough the central point, $f(\hat{x},\hat{y}) = f_0$ at $(\hat{x},\hat{y}) = (0,0)$; thereby avoiding uncertainty regarding the value assigned to the primitive variables during the explicit time integration procedure. Clouds containing seven points (six surrounding points plus the central one) have been used in the work presented in this paper, see Figure 2.

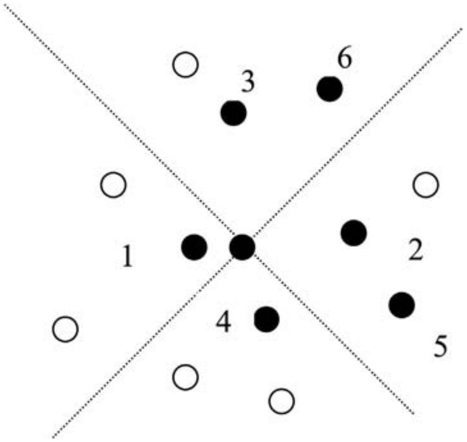

Figure 2.
Typical cloud (black dots) surrounding a central point

The criteria to choose the six surrounding points are as follows:

- The neighbourhood of the central point is inspected to select the closest point to the central one (point 1 in Figure 2).
- Selection of point 1 maps the surrounding region into four sectors, each of them covering a 90° angle. Additional points are selected within the three remaining sectors such that they are closest to the central one (points 2, 3 and 4 in Figure 2).
- Two sectors out of the existing four are chosen at random and one point is selected inside each one that is closest to the central point (points 5 and 6 in Figure 2).

This way to define the cloud presents three advantages:

1. It is ensured that information is gathered all around the central point.
2. The random choice of points 5 and 6 avoids preferred directions in the computation of derivatives.
3. The non-uniformity in the computation of derivatives from cloud to cloud created by the random choice of points 5 and 6, triggers the instability required to star vortex shedding. In this way, there is no need to use artificial means such as, for example, continuously rotating the cylinder or imposing a Taylor vortex in the initial flow field.

The least squares matrix equation that yields the five unknowns λ_1-λ_5 for each variable $(\hat{u}, \hat{v}, \hat{p})$ at each central point in the cloud is:

$$\begin{bmatrix} \sum_{k=1}^{6} \hat{x}_i^2 & \sum_{k=1}^{6} \hat{x}_i \hat{y}_i & \sum_{k=1}^{6} \hat{x}_i^3 & \sum_{k=1}^{6} \hat{x}_i \hat{y}_i^2 & \sum_{k=1}^{6} \hat{x}_i^2 \hat{y}_i \\ \sum_{k=1}^{6} \hat{x}_i \hat{y}_i & \sum_{k=1}^{6} \hat{y}_i^2 & \sum_{k=1}^{6} \hat{x}_i^2 \hat{y}_i & \sum_{k=1}^{6} \hat{y}_i^3 & \sum_{k=1}^{6} \hat{x}_i \hat{y}_i^2 \\ \sum_{k=1}^{6} \hat{x}_i^3 & \sum_{k=1}^{6} \hat{x}_i^2 \hat{y}_i & \sum_{k=1}^{6} \hat{x}_i^4 & \sum_{k=1}^{6} \hat{x}_i^2 \hat{y}_i^2 & \sum_{k=1}^{6} \hat{x}_i^3 \hat{y}_i \\ \sum_{k=1}^{6} \hat{x}_i \hat{y}_i^2 & \sum_{k=1}^{6} \hat{y}_i^3 & \sum_{k=1}^{6} \hat{x}_i^2 \hat{y}_i^2 & \sum_{k=1}^{6} \hat{y}_i^4 & \sum_{k=1}^{6} \hat{x}_i \hat{y}_i^3 \\ \sum_{k=1}^{6} \hat{x}_i^2 \hat{y}_i & \sum_{k=1}^{6} \hat{x}_i \hat{y}_i^2 & \sum_{k=1}^{6} \hat{x}_i^3 \hat{y}_i & \sum_{k=1}^{6} \hat{x}_i \hat{y}_i^3 & \sum_{k=1}^{6} \hat{x}_i^2 \hat{y}_i^2 \end{bmatrix} \begin{bmatrix} \lambda_1 \\ \lambda_2 \\ \lambda_3 \\ \lambda_4 \\ \lambda_5 \end{bmatrix} = \begin{bmatrix} \sum_{k=1}^{6} (f - f_0) \hat{x}_i \\ \sum_{k=1}^{6} (f - f_0) \hat{y}_i \\ \sum_{k=1}^{6} (f - f_0) \hat{x}_i^2 \\ \sum_{k=1}^{6} (f - f_0) \hat{y}_i^2 \\ \sum_{k=1}^{6} (f - f_0) \hat{x}_i \hat{y}_i \end{bmatrix} \qquad (19)$$

Time integration is carried out by using a Lax-Wendroff scheme. To achieve stability wherever the clouds of points are not Cartesian, artificial dissipation terms are added to equations (1)-(3).

Artificial dissipation terms

Broadly speaking, the integration method that we use resembles schemes that are typical of compressible flow simulations; i.e. we do not use the classical staggered spatial interpolation schemes implemented for velocity and pressure that characterize many incompressible flow algorithms. In this way, we achieve a simpler and more flexible formulation although, as a drawback, we need to introduce the second and fourth order artificial dissipation terms that are normally used in compressible flow schemes, Matesanz *et al.* (1998). However, contrary to typical compressible flow algorithms, we implement a second order term only in the pressure evolution equation since the second order viscous terms that appear in the momentum equations are enough to achieve stability in this laminar regime. Regarding the practical implementation of the second and fourth order artificial terms in the algorithm, it is to be said that the finite point spatial integration facilitates this task to a very large extent, as it will be shown in the next paragraphs, so that coding complexity caused by these terms is minimum.

Each artificial dissipation term contains one parameter that needs to be chosen so as to achieve stability while introducing the smallest amount of artificial damping in the flow field. This is why a sensitivity analysis of the results with regard to the artificial dissipation parameters has been performed and the outcome is shown in the sensitivity of the results section. In particular, we found that these parameters are rather general for a reasonably wide scope of different Reynolds numbers, and that the results obtained are fairly insensitive to small variations of the limiting artificial dissipation values.

The second order term $L_2(\hat{p})_i$ added to equation (1) at each central point i is:

$$L_2(\hat{p})_i = \frac{\delta_{2p}}{\Delta\hat{t}} \sum_{k=1}^{4} (\hat{p}_k - \hat{p}_i) \tag{20}$$

where δ_{2p} is an artificial viscosity parameter and $\Delta\hat{t}$ is the integration time step. Note that summation in expression (20) extends only to the first four points in the cloud. We found out that extending summation to the two randomly placed points 5 and 6 within the cloud did not enhance stability and was more costly from the computational standpoint. The fourth order dissipation term $L_4(\hat{p})_i$ is obtained by applying twice the second order term (20):

$$L_4(\hat{p})_i = -\frac{\delta_{4p}}{\delta_{2p}} \sum_{k=1}^{4} (L_2(\hat{p})_k - L_2(\hat{p})_i) \tag{21}$$

where δ_{4p} is an artificial viscosity parameter. Similar fourth order dissipation terms are added to the momentum equations (2) and (3). However, in this case, only one artificial viscosity parameter δ_{4u} is used and, since no second order artificial dissipation term is added to these momentum equations, δ_{2u} is taken to be 1 when formulating operator (21) for velocity components. Summarising, the artificial viscosity terms and parameters that have been introduced are:

- equation (1): $L_2(\hat{p})_i$ and $L_4(\hat{p})_i$. δ_{2p} and δ_{4p};
- equation (2): $L_4(\hat{u})_i$. δ_{4u}; and
- equation (3): $L_4(\hat{v})_i$. δ_{4u}.

This formulation is simpler than the one used previously by Mendez and Velazquez (2004) and it makes up for a faster integration procedure without loss of stability properties. The implementation of fourth order dissipation terns effectively changes the order of equations (1)-(3). This means that an additional set of second order boundary conditions needs to be implemented to ensure the correct algorithm convergence. These boundary conditions are:

$$\frac{\partial L_2(\hat{p})_i}{\partial \hat{n}} = 0, \quad \frac{\partial L_2(\hat{u})_i}{\partial \hat{n}} = 0, \quad \frac{\partial L_2(\hat{v})_i}{\partial \hat{n}} = 0, \text{ at the inflow section} \tag{22}$$

$$\frac{\partial L_2(\hat{p})_i}{\partial \hat{n}} = 0, \quad \frac{\partial L_2(\hat{u})_i}{\partial \hat{n}} = 0, \quad \frac{\partial L_2(\hat{v})_i}{\partial \hat{n}} = 0, \text{ at the outflow section} \tag{23}$$

$$\frac{\partial L_2(\hat{p})_i}{\partial \hat{y}} = 0, \quad L_2(\hat{u})_i = 0, \quad L_2(\hat{v})_i = 0, \text{ at solid vertical walls} \tag{24}$$

$$\frac{\partial L_2(\hat{p})_i}{\partial \hat{x}} = 0, \quad L_2(\hat{u})_i = 0, \quad L_2(\hat{v})_i = 0, \text{ at solid horizontal walls} \tag{25}$$

Relations (24) and (25) can easily be re-written when curved walls are considered. The authors have found that formulation of boundary conditions for the artificial dissipation terms plays an important role in the prediction of unsteady vortex shedding. In particular, imposing $\partial L_2(\hat{u})/\partial \hat{n} = \partial L_2(\hat{v})/\partial \hat{n} = 0$ at curved walls suppressed unsteady vortex shedding completely. In the case of cylinder with sharp corners, vortex shedding occurred both with boundary conditions (24) and (25) and with zero normal derivatives.

Validation results

The formulation presented in the previous section differs from the previous one presented by Mendez and Velazquez (2004) in four main aspects:

1. Six points plus the central one now make up each cloud, and points 5 and 6 are chosen at random.
2. A least squares approximation is selected that passes through the central point.
3. The chosen least squares approximation is not weighted with distances from the cloud points to the central point. In this way, the number of operations to be performed per iteration is diminished and the computational efficiency is increased.
4. In the same spirit, artificial dissipation terms are re-formulated so as to achieve more computational efficiency.

These changes require that, before addressing the problem of predicting local variables in the square cylinder wake, the solver is validated with regard to global aerodynamics coefficients. To perform this validation, we have used results published in the open specialised literature concerning flow around circular and square cylinders in the range of Reynolds numbers spanning from 10 to 200.

Computational parameters for the flow simulation around the circular cylinder are:

- Type of computation: free stream conditions.
- Circular cylinder diameter = 1.
- Computational domain diameter = 60.
- Number of points at the cylinder surface = 720.
- Points inside the computational domain = 34,860.
- Distance from the first point to the cylinder surface = $\pi/720$.
- Artificial compressibility parameter $\beta = 100$.
- Dimensionless time step $\Delta\hat{t} = 1.0 \times 10^{-4}$.
- Artificial viscosity parameters: $\delta_{2p} = 2.0 \times 10^{-2}$, $\delta_{4p} = 8.0 \times 10^{-3}$, $\delta_{4u} = 1.0 \times 10^{-2}$.

Comparison between the average drag Cd_{av}, peak lift Cl_{peak} and Strouhal number S obtained with the finite point solver and the results reported by other researches is presented in Table I as a function of the Reynolds number. The percentage of deviation ε is also given besides each column. Regarding drag, deviations from the measured data (reference A) are always less than 12 percent and they tend to decrease for larger Reynolds numbers. It is to be said that uncertainty in the measurements is larger for the smaller Reynolds numbers. Deviations with regard to other computational work are also smaller than 10 percent except for Reynolds 10 and 40 with reference C. Regarding lift, deviations are, again, smaller than 10 percent except in one of the cases computed by the authors of reference C. It is interesting to notice that in this reference, Ding *et al.* (2004), the authors use a hybrid finite differences – finite point method although their formulation of the continuity equation and the details of the finite point algorithm are quite different from the ones that we use in the present work. Regarding the Strouhal number predictions, deviations are, except in one case that is, again, reference C, always smaller than 5 percent no matter whether experimental or computational results are considered.

Concerning the flow around a square cylinder, computational parameters are as follows:

- Type of computation: free stream conditions.
- Length of the square cylinder side = 1.
- Horizontal dimension of the square shaped computational domain = 60.
- Vertical dimension of the square shaped computational domain = 60.
- Number of points at the cylinder surface = 400.
- Points inside the computational domain = 37,560.
- Distance from the first point to the square cylinder surface = 1/100.
- Artificial compressibility parameter $\beta = 100$.
- Dimensionless time step $\Delta\hat{t} = 1.0 \times 10^{-4}$.
- Artificial viscosity parameters: $\delta_{2p} = 1.2 \times 10^{-2}$, $\delta_{4p} = 1.2 \times 10^{-2}$, $\delta_{4u} = 1.2 \times 10^{-2}$.

Table I.
Circular cylinder results

Re	Ref.	Cd_{av}	ε (percent)	Cl_{peak}	ε (percent)	*S*	ε (percent)
10	Present	2.68					
	A	2.95	9				
	B	2.85	6				
	C	3.00	11				
20	Present	1.98					
	A	2.02	2				
	B	2.05	3				
	C	2.18	9				
40	Present	1.51					
	A	1.60	6				
	B	1.52	1				
	C	1.71	12				
80	Present	1.28		0.22		0.139	
	E					0.141	1
100	Present	1.27		0.32		0.156	
	A	1.26	1				
	C	1.33	5	0.28	14	0.164	5
	D	1.35	6	0.34	6	0.164	5
	E					0.164	5
150	Present	1.26		0.50		0.175	
	D	1.33	5	0.53	6	0.182	4
	E					0.172	2
200	present	1.26		0.64		0.183	
	C	1.33	5	0.60	7	0.196	7
	D	1.31	4	0.69	7	0.192	5
	E					0.183	0

Notes: Comparison of between aerodynamics coefficients (average drag Cd_{av}, peak lift Cl_{peak} and Strouhal number *S*) by using the finite point solver and those provided by other researchers. A – Tritton (1959) experimental, B – Dennis and Chang (1970) numerical, C – Ding *et al.* (2004) numerical, D – Liu *et al.* (1998) numerical, E – Fey *et al.* (1998) experimental. The percentages of deviation between present computed results and the reference results are given under the ε sub-headings

Table II shows the summary of the results obtained together with those reported by other researchers. Regarding drag, our computational results differ from the ones reported in references H and I by a factor less than 10 percent. In particular, the agreement with results provided by Sohankar *et al.* (1997), reference I, is 2 percent at most. Deviations in peak lift and rms are, also, smaller than 13 percent. Nevertheless, the absolute values of Cl_{peak} and Cl_{rms} are small and this fact leads to larger relative deviations. Comparison between our computed Strouhal number results and the experimental data of Davis *et al.* (1984), reference F, and Okajima (1982), reference G, show a deviation of 7 percent at most. Computations have been restricted to Reynolds numbers smaller than 200 because, as shown by Williamson (1996), 3D effects appear beyond this value.

Wake results

To study the capability of the solver to predict local variables in the wake of bluff bodies, the authors generated a series of experimental data for comparison purposes. The experiments were carried out in the low velocity wind tunnel of Instituto Universitario Ignacio da Riva at Universidad Politecnica de Madrid. This open circuit

Re	Ref.	Cd_{av}	ε (percent)	Cl_{peak}	ε (percent)	Cl_{rms}	ε (percent)	S	ε (percent)
100	Present	1.47		0.26		0.18		0.141	
	G							0.136	4
	I	1.48	1			0.16	13	0.146	3
	H	1.61	9	0.27	4			0.154	8
150	Present	1.45		0.39		0.27		0.152	
	H	1.56	7	0.38	3			0.165	8
200	Present	1.47		0.57		0.40		0.151	
	F							0.145	4
	G							0.141	7
	I	1.45	2			0.36	11	0.149	1
	H	1.60		0.62	8			0.157	4

Notes: Comparison of between aerodynamics coefficients (average drag Cd_{av}, peak lift Cl_{peak} and Strouhal number S) by using the finite point solver and those provided by other researchers. F – Davis and Moore (1984) experimental, G – Okajima (1982) experimental, H – Franke *et al.* (1990) numerical, I – Sohankar *et al.* (1997) numerical. The percentages of deviation between present computed results and the reference results are given under the ε sub-headings

Table II.
Square cylinder results

blown-down wind tunnel is characterised by a test section of 100 by 50 mm. Air is propelled by four fans prior to coming into a settling chamber. Before moving to the test section, air passes through a series of devices aiming to make the flow as straight as possible. Test chamber length is 300 mm. Wind velocity ranges from 0.45 to 2.45 m/s and this means that a typical test cylinder having a diameter of 3 mm (6 percent blockage) could be tested from $Re = 90$ up to 500, at room temperatures of the order of 25°C. Turbulence level in the tunnel (rms) was measured to be less that 0.02 m/s at a wind velocity of 0.90 m/s (uncertainty of ± 2 percent). This rms value is defined by, first, subtracting the signal mean from its time series; then, computing the mean of the square of the resulting signal and, finally, taking the root of this value. Uncertainty in the velocity measurements was also ± 2 percent. The hot wire anemometer system was a Dantec Streamline Research CTA system. Probe type was 55P31 with 1 μm Pt and calibration was carried out for velocities up to 3 m/s. The vertical positioning system for the hot wire anemometer moved in steps of 1 mm. The experimental runs were repeated to check that deviations in the gathered data were within acceptable limits. The experimental results presented hereafter (velocity and rms profiles) are the average of the results obtained in the different runs.

The computational parameters were those described and used in the previous section for code validation purposes. The computational domain contained 32,017 points and it reproduced the wind tunnel test section (Figure 3). Three different series of runs were performed at $Re = 110$, 210 and 268. According to Williamson (1996), the $Re = 110$ regime is fully 2D so that the finite point solver fits the flow characteristics. $Re = 210$ describes the regime that occurs right after the onset of 3D effects, although these are expected to be small. Finally, $Re = 268$ is associated to the transitional regime. Therefore, we expect the quality of the 2D simulations to deteriorate steadily when the Reynolds number grows beyond the purely 2D regime.

Velocities and normalized rms ($\hat{u}_{rms}/\hat{u}_{local}$) were measured at three sections downstream of the square cylinder located at $\hat{x}/D = 1, 3$ and 7, respectively, (the origin of co-ordinates is located at the cylinder center). Comparison between measured and

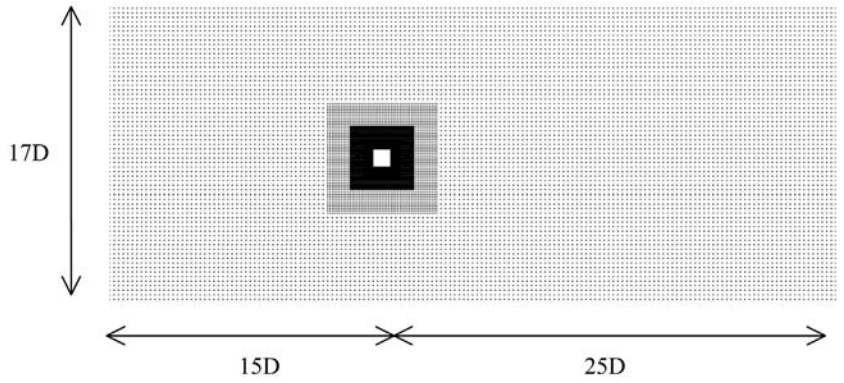

Figure 3.
Computational domain used for wind tunnel simulation runs

computed average absolute velocity $(\hat{u}^2 + \hat{v}^2)^{1/2}$and normalized rms results is shown in Figures 4-6. Computation of average velocity profile and rms was carried out over 100 lift cycles, so uncertainty of the averaging process was ±1 percent.

Re *110*

This is the case with the lowest velocity. The rms signal was so small at the position closer to the base of the cylinder ($x/D = 1$) that that it nearly went below the sensitivity of the data acquisition system (coordinate of the upper right cylinder corner is (x/D, y/D) = (0.5, 0.5)). This is the reason why this specific plot is missing in Figure 4. Regarding prediction of average velocity profiles, maximum deviation between measured data and computed results was 10 percent except at $y/D = 0$. The quality of the predictions improved at sections located farther away from the cylinder. For instance, deviations between measured data and computed results came down to a maximum of 5 percent at $x/D = 7$. The finite point algorithm also appears to resolve the width of the vortex street with a fair accuracy as it could be seen in the left hand side plots of Figure 4. Prediction of rms values is somewhat more difficult than the prediction of an average primitive variable because it involves the computation of a high frequency oscillating value. Nevertheless, the right hand side plots of Figure 4 show that the finite point algorithm is able to predict this variable with a reasonable degree of accuracy. Deviations between measurements and computation were smaller than 5 percent at $x/D = 3$. The fact that the anemometer positioning system moved in steps of 1 mm caused us to miss the point where rms reaches it maximum value in the vortex street. We found out that the point where velocity rms is maximum is located very close to the point where the average absolute vorticity reaches its maximum. Further downstream in the wake ($x/D = 7$) accuracy of the predictions improved. A graphical impression of the uncertainty associated to the experimental data is given in the thick horizontal segments that appear in the upper left and lower right plots of Figure 4.

Re *210*

According to previous results, Williamson (1996), the onset of 3D effects in a square cylinder wake starts at $Re = 198$; then, our $Re = 210$ computation is located just a shade beyond that very point. Prediction of average velocity profiles still proved to be fairly accurate except at the particular point $(x/D, y/D) = (1,0)$, see Figure 5. In general,

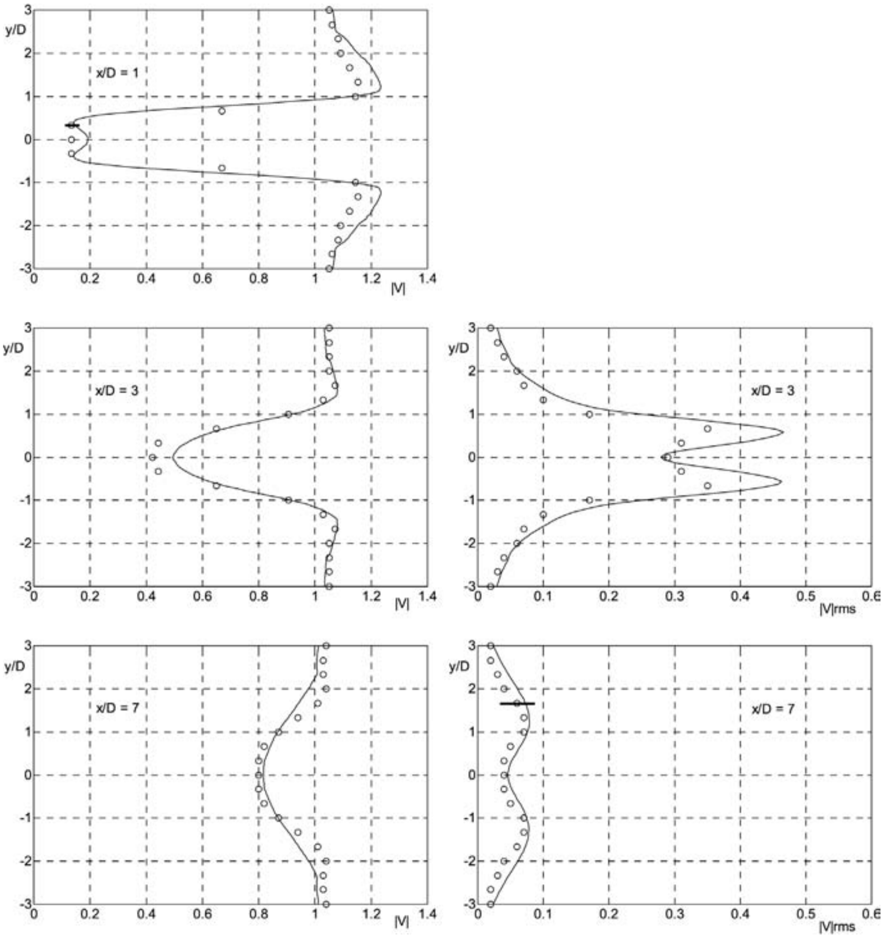

Figure 4.
Reynolds 110. Left: mean values of the absolute velocity $(\hat{u}^2 + \hat{v}^2)^{1/2}$at vertical sections $x/D = 1, 3$ and 7. ∇ experimental data, – computed values. Right: rms absolute velocity at vertical sections $x/D = 3$ and 7. ∇ experimental data, – computed values

deviations between measured and computed data were smaller than 10 percent. Concerning rms, a slight deterioration of the quality of results could be observed when compared with the case $Re = 110$. Deviations, however, were small and this means that the finite point algorithm could be used in this regime for practical application purposes such as the study of MEMS behaviour (see Introduction).

A few points arise when comparing the results obtained for Re 110 and 210. It is significant that velocity profiles at section $x/D = 1$ appear to be much more alike than the profiles at sections $x/D = 3$ and 7. This fact suggests that the local flow field is less dependent on the Reynolds number than the flow further downstream; that is, the local flow field appears to be mostly governed by the geometry. Away from the cylinder, the wake forgets the information about the details of the geometry and its spread is governed by the Reynolds number. Regarding unsteadiness in the velocity field, it is to be noticed that at section $x/D = 3$ the velocity rms at $Re = 110$ is larger than at $Re = 210$. On the contrary, at $x/D = 6$, velocity rms is larger at $Re = 210$. The reason

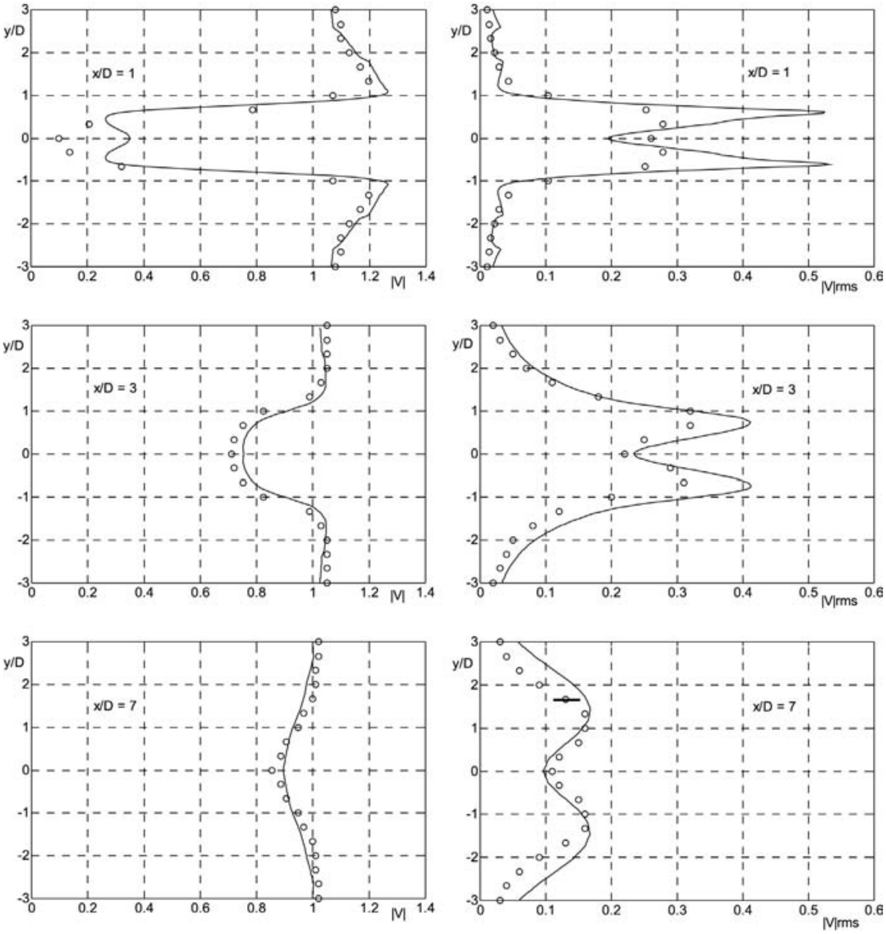

Figure 5.
Reynolds 210. Left: mean values of the absolute velocity $(\hat{u}^2+\hat{v}^2)^{1/2}$at vertical sections $x/D = 1, 3$ and 7. ∇ experimental data, – computed values. Right: rms absolute velocity at vertical sections $x/D = 1$, 3 and 7. ∇ experimental data, – computed values

for this behavior could be that, at $Re = 110$, the perturbations are bigger in the vicinity of the cylinder, but they quickly die away because of the larger viscosity value. In fact, rms values at $x/D = 6$ are two times larger at Reynolds 210 than at $Re = 110$.

Re *268*

According to Williamson (1996), this Reynolds number falls within the so-called transitional regime where bursts of 3D effects suddenly appear and disappear. This is the reason why our 2D results merely reproduce the generic trend of both velocity and rms without providing an acceptable quantitative agreement. It is, nevertheless, interesting to notice that both velocity and rms computed profiles are reasonably accurate at section $x/D = 1$. This fact suggests that the extend of 3D effects is smaller close to the cylinder and grows downstream along the wake (Figure 6).

Concerning the case at $Re = 110$, upper plots of Figure 7 show average pressure and vorticity at vertical sections $x/D = 0.75$, 1.5, 3 and 6, while pressure and vorticity

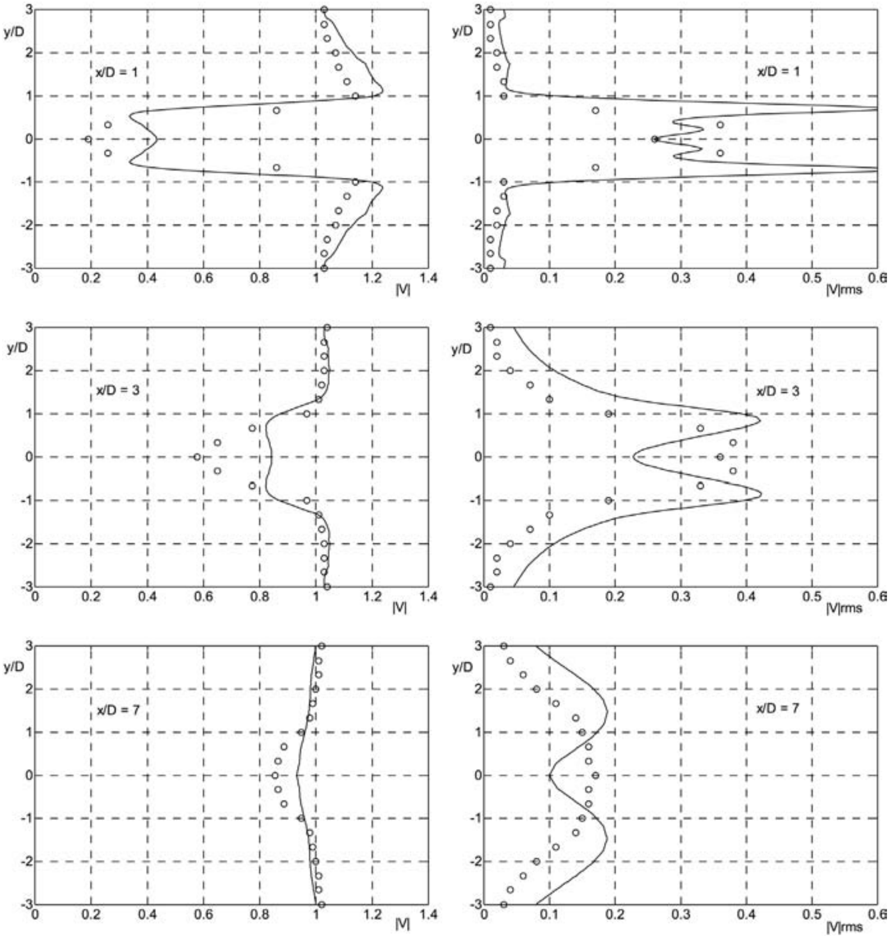

Figure 6.
Reynolds 268. Left: mean values of the absolute velocity $(\hat{u}^2+\hat{v}^2)^{1/2}$at vertical sections $x/D=1, 3$ and 7. ∇ experimental data, – computed values. Right: rms absolute velocity at vertical sections $x/D=1$, 3 and 7. ∇ experimental data, – computed values

contours are presented in the lower plots. An interesting feature of the pressure plot at $x/D=0.75$ is the prediction of a nearly constant pressure in the region spanning $(0.5 \leq y/D \leq 0.5$ that is located right behind the cylinder. This prediction agrees well with the well known fact of the existence of a relatively large, low velocity, nearly constant pressure, flow region behind bluff bodies. Pressure oscillations are small in this region: maximum rms value is 0.12 at the back center line and it decreases towards the corners of the cylinder: rms = 0.08 at both $(x/D, y/D)=(0.75, 0.50)$ and $(x/D, y/D)=(0.75, -0.5)$. Pressure contours shown in the lower left plot of Figure 7 give an impression of the extent of the nearly constant pressure region. Vorticity at the specified sections is presented in the upper right plot of Figure 7, while contours are shown in the lower right plot. Here, it is also possible to discern a region of nearly constant vorticity in the vicinity of the back centerline.

Pressure, absolute value of average velocity $(\hat{u}^2+\hat{v}^2)^{1/2}$ and vorticity along horizontal sections $y/D=0.00$, 0.25, 0.50 and 0.75, are shown in Figure 8.

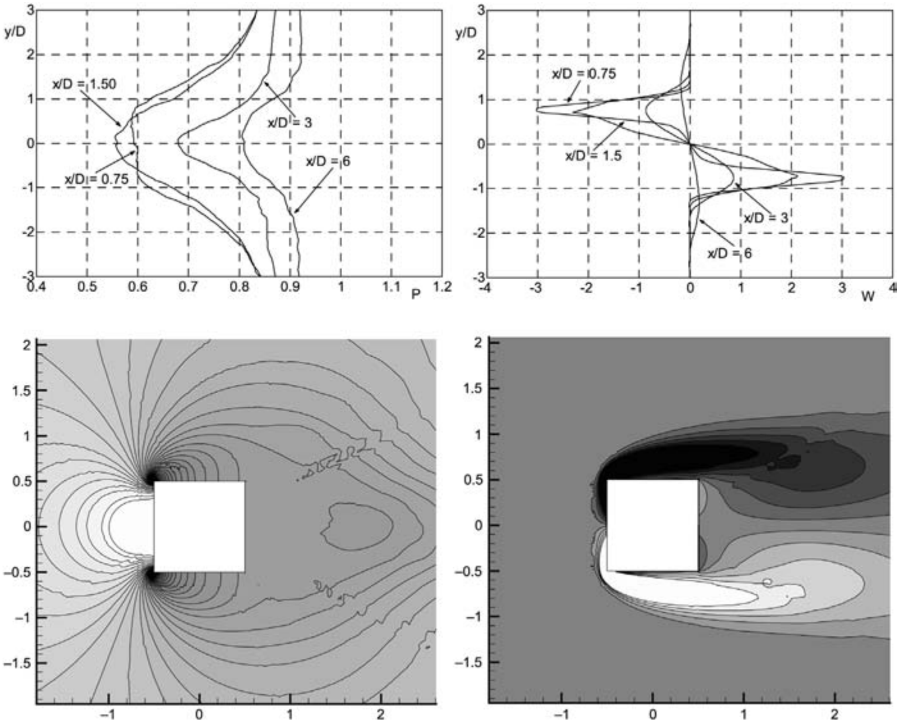

Figure 7.
Reynolds 110. Left: mean pressure at vertical sections $x/D = 0.75$, 1.5, 3 and 6, and average pressure contours around the square cylinder. Right: average vorticity at vertical sections $x/D = 0.75$, 1.5, 3 and 6, and average vorticity contours around the cylinder

Pressure recovery and velocity and vorticity homogenization occur within a horizontal distance of the order of 5-6 cylinder diameters. The average absolute velocity profile at section $y/D = 0.00$ shows a plateau like behavior in the region $1.5 \leq x/D \leq 2.0$. Average velocity grows from the cylinder surface at a fairly constant rate up to $x/D \approx 1.5$; then, it becomes nearly constant up to $x/D \approx 2.0$ before resuming its growth again. The authors were not able to find an explanation for this behavior.

There have been many attempts in the literature to develop models for the prediction of base pressure behind blunt bodies. Most of these models have been developed in the context of aerospace applications and have dealt with high speed turbulent flows, see for example, Rubio *et al.* (2001). The basic assumption that supports these formulations is that there exists a closed cavity behind the blunt body where pressure could be considered to be nearly constant. Net mass balance across the developing shear layers determines the size of the cavity and the base pressure itself. Models that deal with open base flows have also been attempted. Broadly speaking, it could be said that comparison between predictions provided by these models and experimental and numerical data has been reasonably successful. Now, the point is whether it would be feasible to develop a similar type of model for the unsteady laminar regime. In this context, the results shown in Figures 7 and 8 provide a mixed feeling. If we analyze a region whose size is equal to that of the square cylinder and it is located right behind it ($0.5 < x/D < 1.5$, and $-0.5 < y/D < 0.5$) we find that although pressure is certainly not constant, deviations from a mean value are not very large. For instance, at section

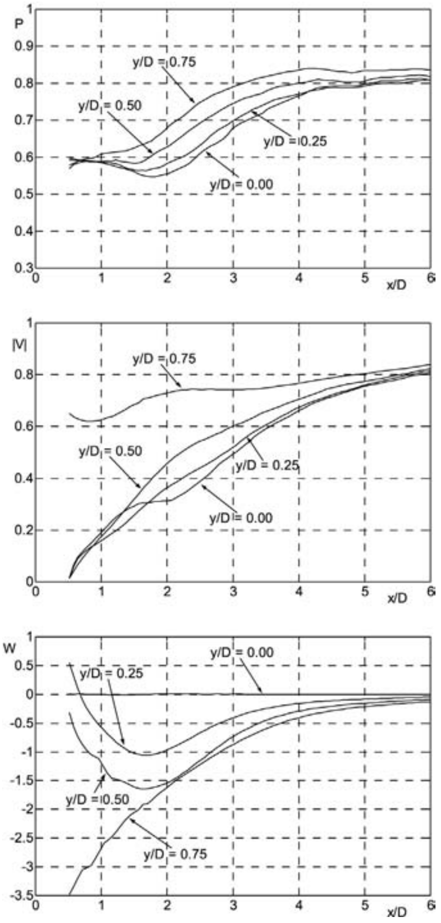

Figure 8.
Reynolds 110. mean pressure, absolute velocity $(\hat{u}^2 + \hat{v}^2)^{1/2}$ and vorticity at horizontal sections $y/D = 0.00$, 0.25, 0.50 and 0.75

$x/D = 0.75$ (Figure 7) pressure is nearly constant, and at section $x/D = 1.5$ pressure deviations from the former value are smaller than 10 percent. In the longitudinal direction (Figure 8) pressure deviations from the mean value are also smaller than 10 percent. However, when looking at the vorticity plots of Figure 7, we find that the thickness of the high vorticity regions is large so that it is not straightforward to devise a zonal model, somehow similar to the ones mentioned previously, that could be used to make fast and accurate predictions of base pressure.

Sensitivity of the results

The sensitivity of the validation results obtained previously has been studied with regard to the computational domain discretisation characteristics and values of the artificial viscosity parameters. In particular, three different grids have been considered from the geometry point of view. All three computational domains were square shaped and had the same vertical and horizontal dimension 60, while the side length of the square cylinder was 1.

1. *Grid 1.* About 196 points at the cylinder surface. About 23,236 points inside the computational domain. Distance from the first point to the cylinder surface equal to 1/49.
2. *Grid 2.* About 304 points at the cylinder surface. About 29,784 points inside the computational domain. Distance from the first point to the cylinder surface equal to 1/76.
3. *Grid 3.* About 400 points at the cylinder surface. About 37,560 points inside the computational domain. Distance from the first point to the cylinder surface equal to 1/100.

The different computations that have been carried out, all of them at the baseline Reynolds number of 200, $\Delta\hat{t} = 1.0 \times 10^{-4}$, $\beta = 100$, and the results obtained are presented in Table III. For each grid, results were converged for diminishing values of the artificial viscosity parameters.

The process was assumed to be finalized when the algorithm failed to converge (FC) because of the very small values of δ_{2p}, δ_{4p} and δ_{4u}. The converged values of the aerodynamics coefficients for each of the grids were as follows:

- Grid 1: $\mathrm{Cd}_{\mathrm{av}} = 1.49$, $\mathrm{Cl}_{\mathrm{peak}} = 0.57$, $S = 0.149$
- Grid 2: $\mathrm{Cd}_{\mathrm{av}} = 1.49$, $\mathrm{Cl}_{\mathrm{peak}} = 0.58$, $S = 0.146$
- Grid 3: $\mathrm{Cd}_{\mathrm{av}} = 1.47$, $\mathrm{Cl}_{\mathrm{peak}} = 0.57$, $S = 0.151$

Deviations between these values were 1 percent for $\mathrm{Cd}_{\mathrm{av}}$, 2 percent for $\mathrm{Cl}_{\mathrm{peak}}$, and 3 percent for S, so we could assume that the results are converged with regard to computational domain discretization and artificial viscosity parameters.

To assess the effect of the time step, we performed two additional computations by changing the time step, $\Delta\hat{t} = 1.0 \times 10^{-4}$, of case 23 (Table III) that we took as a baseline for this specific purpose. Time step for additional cases 31 and 32 were

Table III.
Results of the computational cases that have been performed for the sensitivity analysis with regard to cylinder and computational domain discretisation, and artificial viscosity parameters

Case	Grid	δ_{2p}	δ_{4p}	δ_{4u}	$\mathrm{Cd}_{\mathrm{av}}$	$\mathrm{Cl}_{\mathrm{peak}}$	$\mathrm{Cl}_{\mathrm{rms}}$	S
1	1	1.0×10^{-2}	4.0×10^{-3}	4.0×10^{-3}	1.56	0.54	0.39	0.146
2	1	5.0×10^{-3}	2.0×10^{-3}	2.0×10^{-3}	1.54	0.56	0.41	0.150
3	1	2.5×10^{-3}	1.0×10^{-3}	1.0×10^{-3}	1.52	0.57	0.41	0.150
4	1	1.7×10^{-3}	6.7×10^{-4}	6.7×10^{-4}	1.51	0.57	0.41	0.150
5	1	1.3×10^{-3}	5.0×10^{-4}	5.0×10^{-4}	1.49	0.57	0.41	0.149
6	1	6.3×10^{-4}	2.5×10^{-4}	2.5×10^{-4}	FC	FC	FC	FC
11	2	1.0×10^{-2}	1.0×10^{-2}	1.0×10^{-2}	1.49	0.47	0.34	0.150
12	2	7.5×10^{-3}	7.5×10^{-3}	7.5×10^{-3}	1.49	0.47	0.34	0.149
13	2	5.0×10^{-3}	5.0×10^{-3}	5.0×10^{-3}	1.48	0.52	0.37	0.147
14	2	3.8×10^{-3}	3.8×10^{-3}	3.8×10^{-3}	1.48	0.54	0.37	0.146
15	2	2.5×10^{-3}	2.5×10^{-3}	2.5×10^{-3}	1.49	0.58	0.40	0.146
16	2	1.3×10^{-3}	1.3×10^{-3}	1.3×10^{-3}	FC	FC	FC	FC
21	3	8.0×10^{-3}	2.0×10^{-2}	2.0×10^{-2}	1.46	0.47	0.33	0.147
22	3	4.0×10^{-3}	1.0×10^{-2}	1.0×10^{-2}	1.48	0.50	0.35	0.150
23	3	2.0×10^{-3}	5.0×10^{-3}	5.0×10^{-3}	1.48	0.54	0.37	0.151
24	3	1.0×10^{-3}	2.5×10^{-3}	2.5×10^{-3}	1.47	0.56	0.39	0.151
25	3	5.0×10^{-4}	1.3×10^{-3}	1.3×10^{-3}	1.47	0.57	0.40	0.151
26	3	2.5×10^{-4}	6.3×10^{-4}	6.3×10^{-4}	FC	FC	FC	FC

$1.0 \times 10^{-4} \times 2$ and $1.0 \times 10^{-4}/2$, respectively. To perform a fair comparison between these three cases, artificial viscosity parameters were modified to ensure that the following groups remained invariant:

$$\frac{\delta_{2p} d^2}{\Delta\hat{t}}, \quad \frac{\delta_{4p} d^4}{\Delta\hat{t}}, \quad \text{and} \quad \frac{\delta_{4u} d^4}{\Delta\hat{t}} \tag{26}$$

It is to be noted that the artificial viscosity term described in relation (20) has a pseudo-Laplacian form. Therefore, the parametric groups (26), where d is a typical distance within the cloud, describe the order of magnitude of these artificial terms. Results obtained for the three computations are as follows:

- Case 23: $\mathrm{Cd}_{\mathrm{av}} = 1.48$, $\mathrm{Cl}_{\mathrm{peak}} = 0.54$, $S = 0.151$
- Case 31: $\mathrm{Cd}_{\mathrm{av}} = 1.48$, $\mathrm{Cl}_{\mathrm{peak}} = 0.53$, $S = 0.152$
- Case 32: $\mathrm{Cd}_{\mathrm{av}} = 1.47$, $\mathrm{Cl}_{\mathrm{peak}} = 0.53$, $S = 0.152$

Deviations were 1 percent for $\mathrm{Cd}_{\mathrm{av}}$, 2 percent for $\mathrm{Cl}_{\mathrm{peak}}$, and 1 percent for S, so we could conclude that the results are also converged with regard to the computational time step. Finally, sensitivity of the local flow variables and rms values has been addressed. In particular, results corresponding to cases 22, 23 and 24 (Table III) were used for comparison. Figure 9 shows the average absolute velocity values and rms's for these three computational cases at three sections ($x/D = 1$, 3 and 6) away from the cylinder. Regarding velocity profiles, maximum deviations occur in the region close to the back centerline. In the worst case, $x/D = 3$, deviations in this specific region are smaller than 5 percent. Away from the centerline, results associated to cases 22, 23 and 24 are virtually indistinguishable. Regarding rms profiles, the worst case occurs at $x/D = 6$ and $y/D = 1$. In this case, maximum deviations are, again, smaller than 5 percent. Away from this local spot, rms values coincide for the three cases that have been computed.

Regarding the pressure boundary condition at the cylinder walls, three different formulations are possible.

Boundary condition A. This is the more exact one, and it consists on solving the one-sided momentum equation at a point close to the cylinder surface. This formulation accounts for the effect of convective terms on the pressure filed at the wall. The practical way to implement it is to solve the appropriate momentum equation at a virtual point located half way between the surface and the first point away from it. For instance, if we consider a horizontal surface, the discretized momentum equation (27) is to be solved at point $(i, j + \frac{1}{2})$, see Figure 10, to yield the sought values of $\hat{p}^{n+1}_{(i,j)}$:

$$\frac{\hat{v}^{n+1}_{(i,j+1)} - \hat{v}^{n}_{(i,j+1)}}{2\Delta\hat{t}} + \frac{\hat{u}^{n+1}_{(i,j+1)}}{2}\,\frac{1}{2}\left(\frac{\partial\hat{v}}{\partial\hat{x}}\right)^{n+1}_{(i,j+1)} + \frac{\hat{v}^{n+1}_{(i,j+1)}}{2}\,\frac{\hat{v}^{n+1}_{(i,j+1)}}{\Delta\hat{y}}$$

$$= -\frac{\hat{p}^{n+1}_{(i,j+1)} - \hat{p}^{n+1}_{(i,j)}}{\Delta\hat{y}} + \frac{1}{Re}\left(\frac{1}{2}\,\frac{\partial^2\hat{v}}{\partial x^2} + \frac{\partial^2\hat{v}}{\partial y^2}\right)^{n+1}_{(i,j+1)} \tag{27}$$

Computation of the different terms in boundary condition (26) is straightforward by using the finite point approximation at point (i, j). The time derivative is computed by using the flow field variables at the previous time step n.

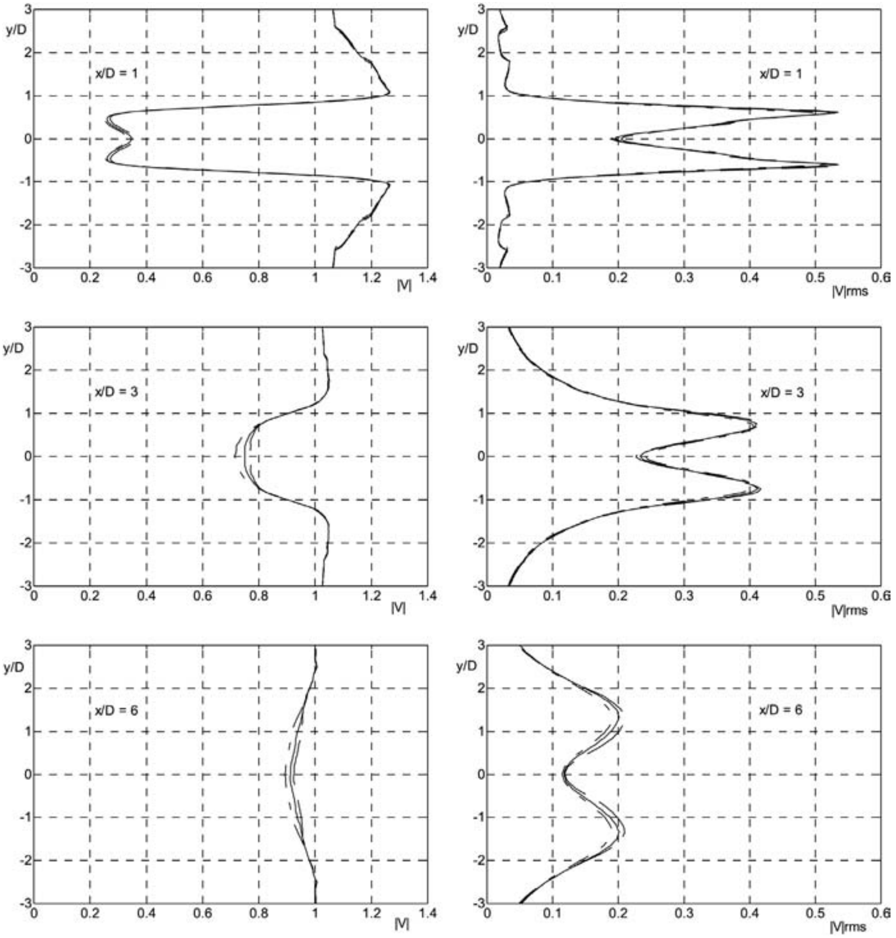

Figure 9.
Sensitivity analysis of the local flow results obtained in the cylinder wake at Reynolds 200. - case 23, -- case 24, - ∇ case 22

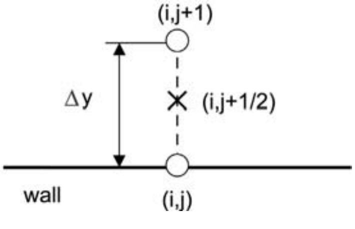

Figure 10.
Node arrangement for implementation of the pressure boundary condition A at the wall

Boundary condition B. This is the one that we have actually used in the work described in this paper, see equation (16). Basically, it represents the limit of previous boundary condition A when the momentum equation is solved at the wall, and all velocities are taken to be zero.

Boundary condition C: It goes a step further from boundary condition B since, due to the high value of the Reynolds number, the dimensionless viscous stress is assumed to be much smaller than the pressure gradient. In practice, this boundary condition reduces to assuming that pressure gradient normal to a wall is zero.

A sensitivity analysis has been performed regarding the choice of the pressure boundary condition. In particular, boundary conditions A and B have been used to solve a case with $Re = 150$. All the other computational parameters were the same as those used in the Wake results section. The global aerodynamics coefficients that we computed were:

Results obtained with boundary condition A

- Cd $= 1.461 \pm 0.022$
- $\mathrm{Cl}_{\mathrm{peak}} = 0.375$
- $S = 0.151$

Results obtained with boundary condition B

- Cd $= 1.455 \pm 0.021$
- $\mathrm{Cl}_{\mathrm{peak}} = 0.379$
- $S = 0.151$

That is, differences in the aerodynamics coefficients were smaller than 1 percent. Now, local profiles of horizontal and vertical velocity, as well as rms values, are compared in Figure 11 at three different section downstream of the cylinder ($x/D = 1$, 3 and 6). Again, the results obtained by using either boundary condition were virtually the same. The reason could be that at Reynolds numbers of the order of 100, velocities close to the surface are not high enough for the convective terms to influence significantly the pressure gradient at the wall.

Conclusions

- The version of the finite point algorithm presented in this paper has evolved, from a previous one, in the direction of improving computational efficiency (by a factor of approximately 20 percent) while keeping prediction accuracy. The driving idea has been to make the algorithm amenable for practical industrial applications in MEMS design. The reason is that to achieve an efficient behavior of these devices, knowledge is required not only of global quantities, such as forces, but also of local values of the unsteady variables.
- The compromises that we have made to achieve better computational efficiency (cloud re-definition, finite point algorithm re-formulation, and artificial dissipation terms re-formulation) did not seem to affect significantly the accuracy of the results obtained, both at the global and the local level. In particular, the flow solver has been applied to predict both global aerodynamics coefficients and experimental local velocity and rms profiles in a square cylinder wake. The results obtained show a reasonable degree of accuracy in both cases (almost always smaller than 10 percent).

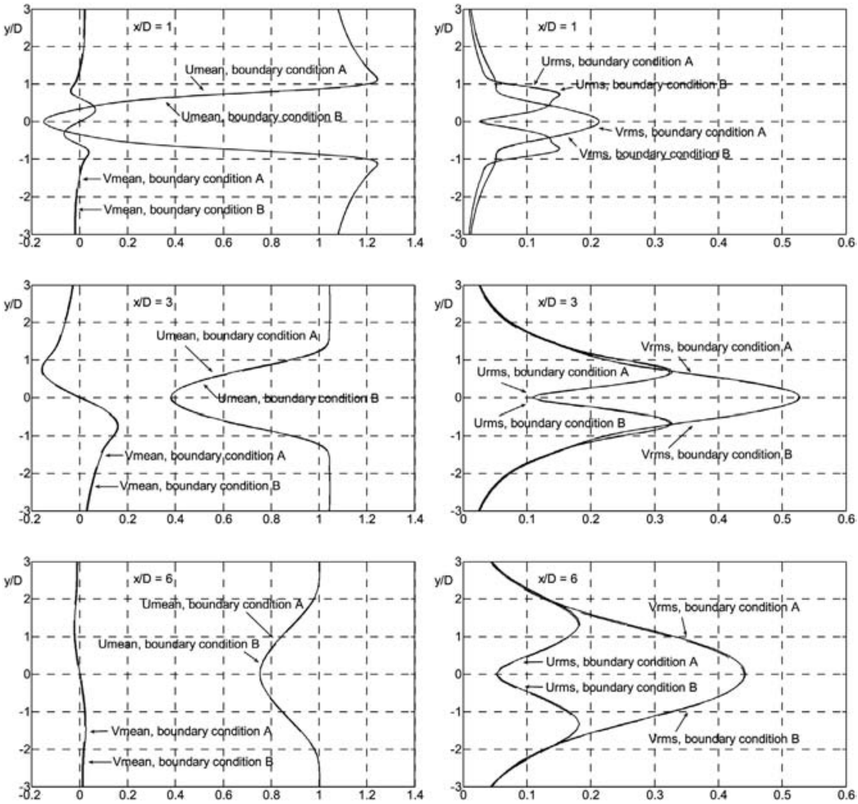

Figure 11.
Reynolds 150. Left: Comparison between mean horizontal and vertical velocity profiles for boundary conditions A (-) and B (--) at three different sections *x*/*D* = 1, 3 and 6 downstream of the cylinder. Left: Comparison between rms horizontal and vertical velocity profiles for boundary conditions A (-) and B (--) at three different sections *x*/*D* = 1, 3 and 6 downstream of the cylinder

- On the numerical side, the sensitivity study that has been performed suggests that the formulation is rather robust and this fact, again, points in the direction of using the solver for industrial purposes. In particular, sensitivity of the results has been studied with regard to cylinder and computational domain discretisation, values of the artificial viscosity parameters and computational time step. In all cases, for a range of Reynolds numbers, it was found that results showed a plateau-like behavior with regard to the selected parameters that points in the direction of an acceptable numerical robustness.
- Finally, it has been shown that appropriate formulation of higher order boundary conditions for the artificial dissipation terms is needed to get correct predictions in this type of laminar, incompressible, unsteady flow problems.

References

Batina, J.T. (1992), "A gridless Euler/Navier Stokes solution algorithm for complex two dimensional applications", NASA Technical Memorandum 107631.

Chorin, A.J. (1967), "A numerical method for solving incompressible viscous flow problems", *Journal of Computational Physics*, Vol. 2, pp. 12-26.

Chung, C.H. (2005), "Numerical simulation of low speed gas flows in a microfluidics system", *Journal of Thermophysics and Heat Transfer*, Vol. 19 No. 3, pp. 336-42.

Davis, R.W., Moore, E.F. and Purtell, L.P. (1984), "A numerical experimental study of confined flow around rectangular rectangles", *Physics of Fluids*, Vol. 27, pp. 46-59.

Dennis, S.R.C. and Chang, G.Z. (1970), "Numerical solutions for steady flow past a circular cylinder at Reynolds number up to 100", *Journal of Fluid Mechanics*, Vol. 42, pp. 471-89.

Ding, H., Shu, C., Yeo, K.S. and Xu, D. (2004), "Simulation of incompressible viscous flows past a circular cylinder by hybrid FD scheme and meshless least square-based finite difference method", *Computer Methods in Applied Mechanics and Engineering*, Vol. 193, pp. 727-44.

Fey, U., Koning, M. and Eckelmann, H. (1998), "A new Strouhal-Reynolds number relationship for the circular cylinder in the range $47 < Re < 2\ 10^5$", *Physics of Fluids*, Vol. 10, pp. 1547-9.

Franke, R., Rodi, W. and Schönung, B. (1990), "Numerical calculation of laminar vortex shedding flow past cylinders", *Journal of Wind Engineering and Industrial Aerodynamics*, Vol. 35, pp. 237-57.

Jensen, P.S. (1972), "Finite difference techniques for variable grids", *Computers & Structures*, Vol. 2, pp. 17-29.

Kiris, C. and Kwak, D. (2002), "Aspects of unsteady incompressible flow simulations", *Computers & Fluids*, Vol. 31, pp. 627-38.

Li, G. and Aluru, N.R. (2002), "Boundary cloud method: a combined scattered point/boundary integral approach for boundary-only analysis", *Computer Methods in Applied Mechanics and Engineering*, Vol. 91, pp. 2337-70.

Liszka, T. and Orkisz, J. (1980), "The finite difference method at arbitrary irregular grids and its application in applied mechanics", *Computers & Structures*, Vol. 11, pp. 83-95.

Liu, C., Zheng, X. and Sung, C.H. (1998), "Preconditioned multigrid methods for unsteady incompressible flows", *Journal of Computational Physics*, Vol. 139, pp. 35-57.

Luo, Y. and Haussler-Combe, U. (2002), "A generalised finite difference method based on minimising global residual", *Computer Methods in Applied Mechanics and Engineering*, Vol. 191, pp. 1421-38.

Matesanz, A., Velazquez, A., Jimenez, A. and Rodríguez, M. (1998), "Numerically robust 3-D finite element Reynolds Averaged Navier Stokes solver for the study of turbulent supersonic external flows", *Computer Methods in Applied Mechanics and Engineering*, Vol. 159, pp. 383-94.

Mendez, B. and Velazquez, A. (2004), "Finite point solver for the simulation of 2-D laminar incompressible unsteady flows", *Computer Methods in Applied Mechanics and Engineering*, Vol. 193, pp. 825-48.

Okajima, A. (1982), "Struhal number of rectangular cylinders", *Journal of Fluid Mechanics*, Vol. 123, pp. 379-98.

Onate, E., Idelsohn, S., Zinkiewicz, O., Taylor, R. and Sacco, C. (1996), "A stabilised finite point method for analysis of fluid mechanics problems", *Computer Methods in Applied Mechanics and Engineering*, Vol. 139, pp. 315-46.

Perrone, N. and Kao, R. (1975), "A general finite difference method for arbitrary meshes", *Computers & Structures*, Vol. 5, pp. 45-7.

Rogers, S.E., Kwak, D. and Kiris, C. (1991), "Steady and unsteady solutions of the incompressible Navier-Stokes equations", *AIAA Journal*, Vol. 29 No. 4, pp. 603-10.

Rubio, G., Matesanz, A. and Velazquez, A. (2001), "Base drag prediction with plume-on including 3-D and real gas effects", *Journal of Spacecraft and Rockets*, Vol. 38 No. 2.

Sohankar, A., Norberg, C. and Davidson, L. (1997), "Numerical simulation of unsteady flow around a rectangular two-dimensional cylinder at incidence", *Journal of Wind Engineering and Industrial Aerodynamics*, Vol. 69, pp. 189-201.

Stone, H.A., Stroock, A.D. and Ajdari, A. (2004), "Engineering flows in small devices. Microfluidics toward lab-on-a-chip", *Annual Review of Fluid Mechanics*, Vol. 36, pp. 381-411.

Tritton, D.J. (1959), "Experiments on the flow past a circular cylinder at low Reynolds numbers", *Journal of Fluid Mechanics*, Vol. 6, pp. 547-67.

Van Male, P., de Croon, M.H.J.M., Tiggelaar, R.M. and Van den Berg, A. (2004), "Heat and mass transfer in a square microchannel with asymmetric heating", *International Journal of Heat and Mass Transfer*, Vol. 47, pp. 87-99.

Williamson, C.H.K. (1996), "Vortex dynamics in the cylinder wake", *Annual Review of Fluid Mechanics*, Vol. 28, pp. 477-539.

Corresponding author
A. Velazquez can be contacted at: avelazquez@aero.upm.es